

CHEMICAL SCIENCES

Chemical Crystallography

Time Resolved Experiments

The moving image-plate system at X7B has proved extremely productive, with a wide variety of reactions and phase transitions studied. This system has been developed to the point where it routinely provides large quantities of high-quality data, too much to be listed here. For details the reader is encouraged to browse the relevant abstracts. Whereas those experiments relate to the conversion between various crystal structures, there are other important structural problems which are interesting when addressed in the time domain. Many small angle scattering experiments on polymers made use of time-resolved data sets.

One other example, with much faster time resolution, is an experiment on the electrodeposition of Cu on Pt(111), performed on X20A by A. Finnefrock *et al.* (Cornell U.). In that work, the Cu is electrodeposited on the Pt surface within 0.02 second after a step in the applied potential, but the overlayer structure requires from 2 to 5 seconds to develop long-range order. More detailed studies of this phenomena should lead to interesting information about the mass-transfer of ions near the electrode surface and other aspects of the deposition process.

Single Crystals

The brightness of synchrotron radiation can be very favorably combined with the use of image plate detectors for structural studies with relatively small single crystal samples. Mentioned here are a few characteristic examples. A. M. Andersen *et al.* (Odense U.), used $25 \times 25 \times 50 \mu\text{m}^3$ crystals at beamline X7B to solve the structure of $\text{Zr}(\text{HPO}_4)_2$. At the same station, T. Jensen *et al.* (Odense U.), solved the structure of $\alpha\text{LiZnAsO}_4$ from a crystal of $17 \times 17 \times 60 \mu\text{m}^3$

and of δLiZnPO_4 from a crystal of $39 \times 16 \times 18 \mu\text{m}^3$.

The image plate technique has application to crystallographic problems with normal-sized crystals as well. P. Coppens *et al.* (SUNY @ Buffalo), have been working on techniques to extract the best-quality intensities from image plates, and extending the limits of electron density analysis. For example, using a $\text{Cr}(\text{NH}_3)_6\text{Cr}(\text{CN})_6$ crystal of $80 \times 30 \times 30 \mu\text{m}^3$ and an x-ray wavelength of 0.394 \AA , they have collected and analyzed data out to 0.25 \AA resolution. B. Iversen *et al.* (U. of California @ Santa Barbara), have extracted the electron density (rather than only the atomic positions) of the actinide $\text{Th}(\text{S}_2\text{P}(\text{CH}_3)_2)_4$ from data taken at X3A1. They avoided the problem of dominance of the heavy Th atom by collecting reflections for which the Th ion core did not contribute. By this means they could determine the charge density, rather than merely atom positions quite readily. Other image plate based studies on X3A by A. Darovsky (SUNY @ Buffalo) include anomalous scattering measurements of mixed valence Mn compounds, resolving the Mn^{2+} - Mn^{3+} thermal equilibrium vs. temperature, and separation of Mn^{3+} and Mn^{4+} sites in two different mixed valence compounds. Both the above studies benefitted from a new technique for extracting unbiased integrated intensities from the image plate data (called the seed-skewness method, R. Bolotovskiy and P. Coppens (SUNY @ Buffalo). It relies on the statistical properties of noise to

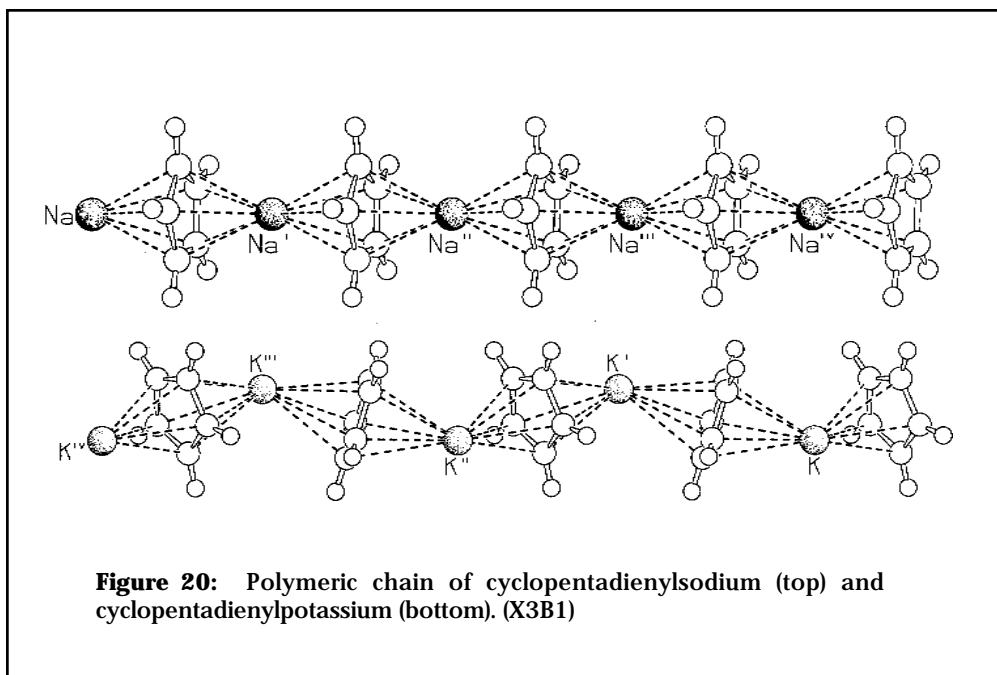


Figure 20: Polymeric chain of cyclopentadienylsodium (top) and cyclopentadienylpotassium (bottom). (X3B1)

isolate the data region corresponding to a diffraction spot (i.e. a region which is not noise).

J. Parise *et al.* (SUNY @ Stony Brook), have used image plate techniques on beamline X3A1 to solve the structures of several new open framework compounds, e.g., GeS_2 and $[(\text{C}_6\text{H}_{13}\text{N}_2)_2(\text{H}_3\text{O})(\text{H}_2\text{O})][\text{AgGe}_4\text{S}_{10}]$ with quite small samples, on the order of 30 microns.

Powder Studies

For many materials, single crystals are simply not available, and one must resort to powder diffraction data for whatever structural information is to be gleaned. Some of the (conceptually) simplest organic salts, like alkali cyclopentadienides AC_5H_5 (A=Li, Na, K, Rb) are sufficiently unstable that single crystals cannot be prepared, but they are of particular interest because theoretical calculations are unable to reproduce the observed structures of related, but more complicated molecules, e.g., $\text{M}(\text{C}_5\text{H}_5)_2$ (M=Be, Mg, Ca). R. Dinnebier (U. Bayreuth) and collaborators have solved a number of these compounds, purely from powder diffraction data at beamline X3A1. In one noteworthy example, they solved the structures of two polymorphs of RbC_5H_5 present in one sample from a single powder pattern. They found that the chains buckled to a different degree as a function of cation size (Figure 20).

Electron Spectroscopy

Valence Electron Excitations

The gas phase research on Beamline U11 has addressed the thermochemistry and spectroscopy of bromine oxides and chlorine oxides with photoionization mass spectrometry. These oxides are not well understood because they have low thermal stability and are difficult to obtain in a pure state. Br_2O has been prepared via the reaction of bromine vapor on solid mercuric oxide. Figure 21(a) shows the first direct determination of the photoionization efficiency (PIE) spectrum of Br_2O . The experimental ionization threshold is in good agreement with the only published value of 10.23 eV from an *ab initio* calculation. The heat of formation of Br_2O can be determined using the appearance energy (AE) of BrO^+ shown in Figure 21(b), together with the previously determined ionization energy of BrO and tabulated heats of formation of BrO and Br . The 0 K value of 124.1 ± 3.5 kJ mol^{-1} thus determined has been selected and cited in the latest NIST-JANAF Thermochemical Tables for the Bromine Oxides. Discharge flow photoionization mass spectrometry has also been used to obtain the PIE spectrum of Cl_2O , ClO radical, the AE of ClO^+ , and a value for the heat of formation of Cl_2O .

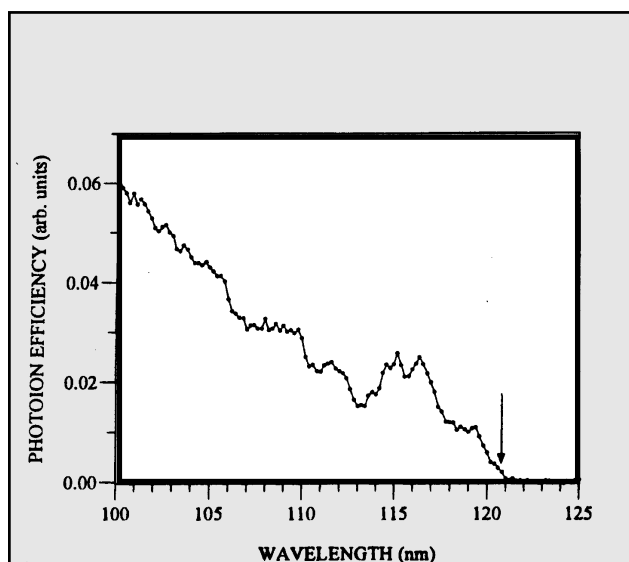
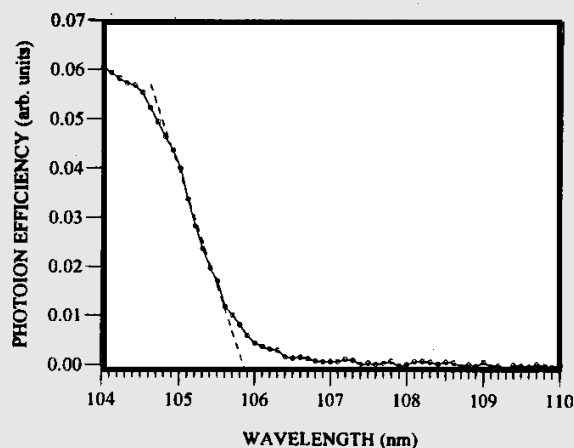
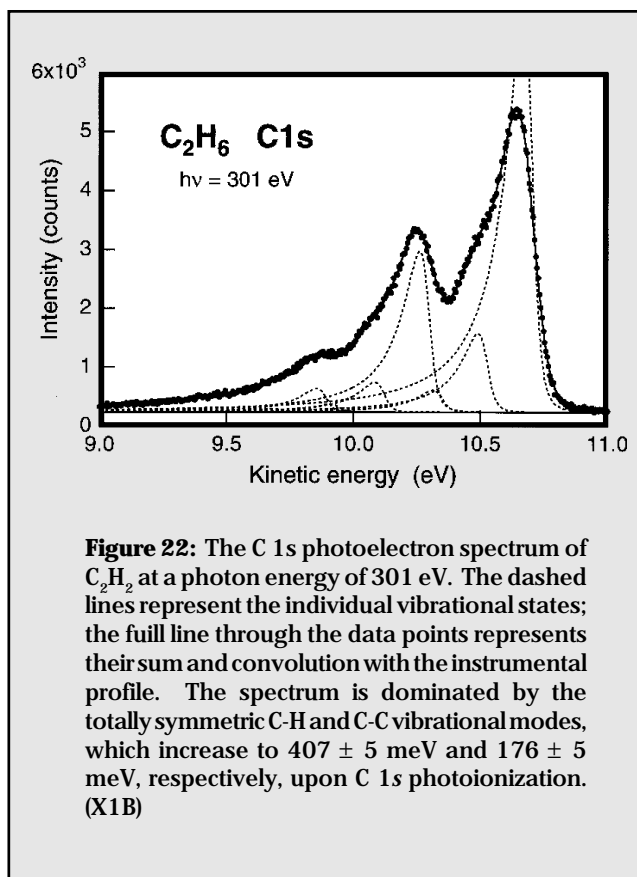


Figure 21: (a) Photoionization efficiency spectrum of Br_2O at a nominal resolution of 0.13 nm. The arrow indicates the onset of ionization at a wavelength of 120.8 nm, yielding an ionization energy 10.26 ± 0.01 eV. (U11)



(b) Photoionization threshold region for the appearance of BrO^+ via the dissociative ionization of Br_2O , at a nominal resolution of 0.13 nm. The linear extrapolation of the spectrum to the baseline yields an onset at 105.84 nm corresponding to an appearance energy of 11.71 ± 0.01 eV.



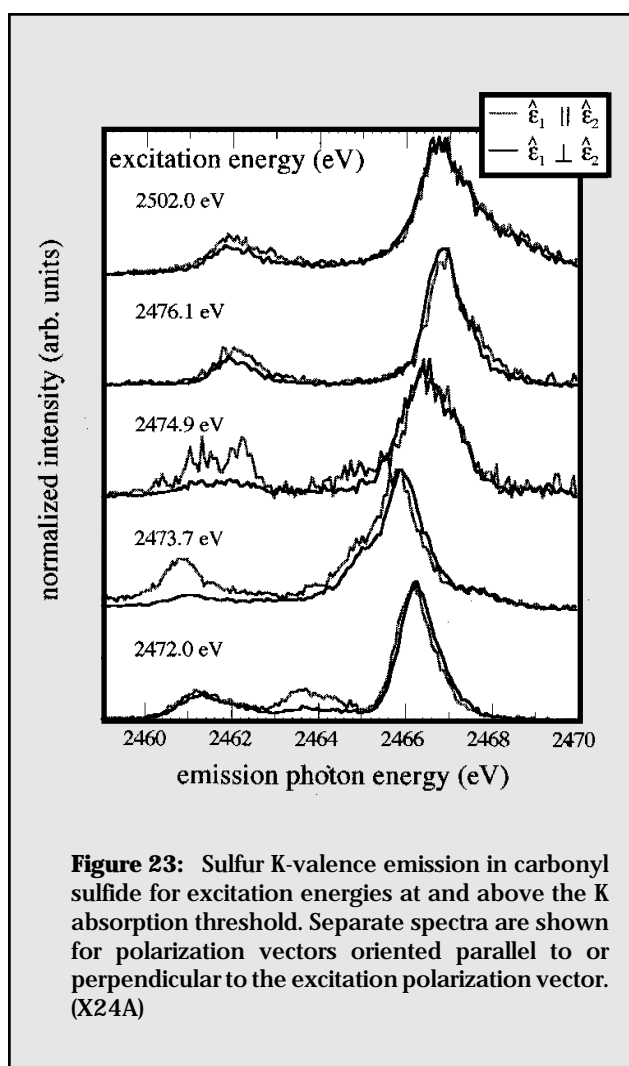
Core Electron Excitations

The interest in atomic-site-selective core-electron excitation at Beamline U15 has been extended to 5-Oxohexanenitrile isolated in D_2 matrices. *In situ* infrared spectroscopy is used to monitor the C-O and the C-N stretches at excitation energies corresponding to the C, N and O resonances and continuum. One of the most interesting results from preliminary experiments is that excitation at resonances, resulting in autoionization producing a single valence hole, favors the photodissociation of carbonyl groups while nitrile group photodissociation is favored by continuum excitation resulting in Auger decay producing a doubly charged molecular ion.

As a continuation of the high-resolution studies of dynamic effects in core excitation on Beamline X1B, the complex vibrational structure in the C 1s photoelectron spectrum of ethane has been studied as the prototype for the alkanes. **Figure 22** shows a least-squares-fit of the vibrational structure. The vibrational energies of the C-H stretch and the C-C stretch are found to increase significantly upon ionization. The bond lengths are also found to be reduced by 0.036 Å for C-H and 0.043 Å for C-C. These and other results on alkenes contribute to the discussion on the correlation between shape resonances

and bond lengths. Furthermore, the recent grating upgrade has enabled the vibrational fine structure in the O 1s photoelectron spectrum in CO_2 to be measured for the first time. It is observed that the antisymmetric C-O stretch mode (307 ± 3 meV) is dominant, as predicted for the lowering of symmetry and core orbital-vibronic coupling upon O 1s core ionization.

On Beamline X24A, polarization-dependent resonant x-ray emission has been studied with excitation at the sulfur K absorption threshold in carbonyl sulfide. **Figure 23** shows the sulfur K-valence emission for different polarizations, at excitation energies for 1s transitions to the lowest unoccupied molecular orbitals, Rydberg states and the continuum. The emission line shape and its differences with respect to the post-threshold emission spectrum are explained by *ab initio* calculations of the intermediate and final state energies. Variations with polarization are explained by a dipole model of absorption and emission.



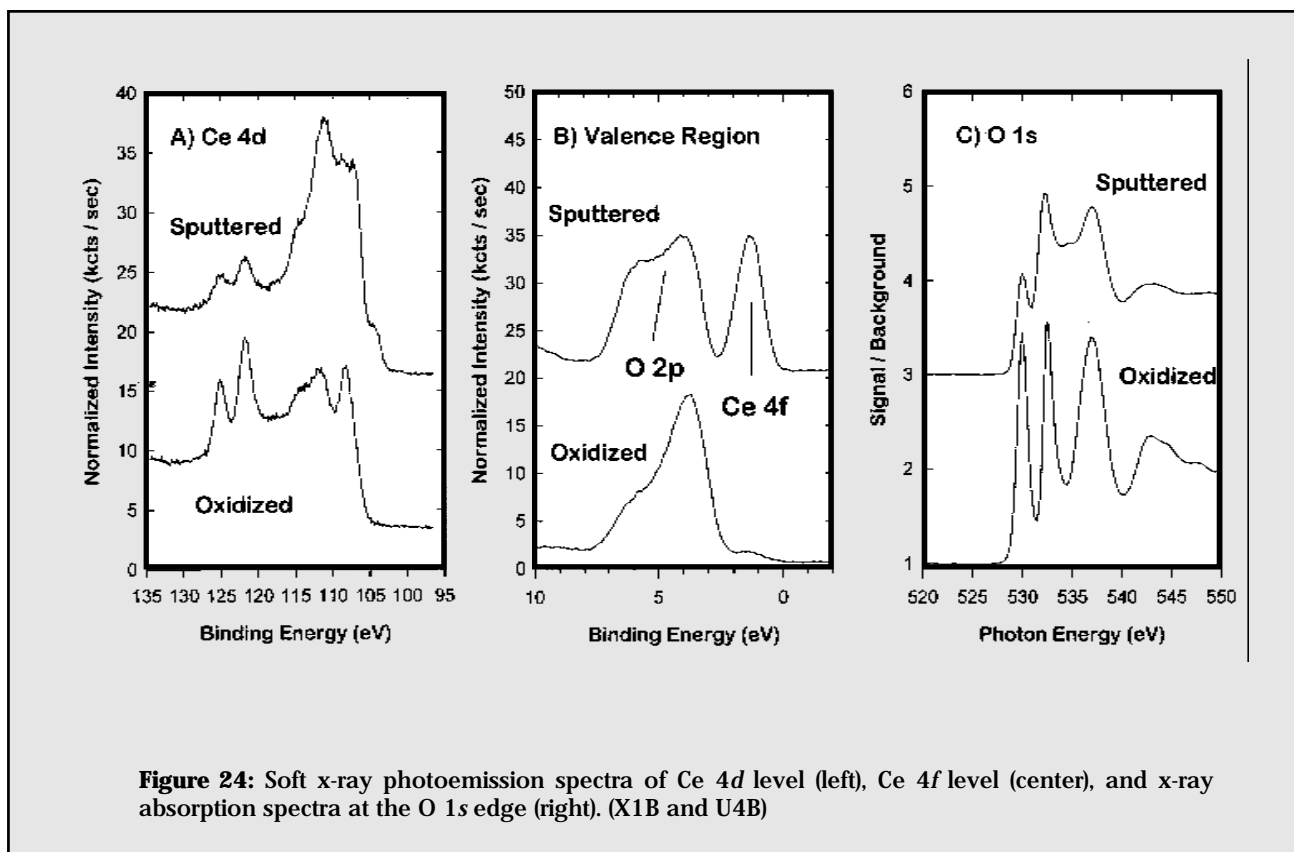


Figure 24: Soft x-ray photoemission spectra of Ce 4d level (left), Ce 4f level (center), and x-ray absorption spectra at the O 1s edge (right). (X1B and U4B)

Photoemission and Photoabsorption from Rare Earth Oxides

The surface chemistry group at Oak Ridge National Laboratory (D. Mullins, D. Huntley and S. Overbury) has begun a series of investigations to study the properties of metals supported on metal oxides. In the initial investigations, the ORNL group has used single crystal films of CeO_2 produced by laser ablation that are ~ 5000 Å thick. CeO_2 is used to enhance the performance of environmental control catalysts such as automotive catalytic converters. The films are highly oriented as indicated by x-ray diffraction, transmission electron microscopy and low energy ion scattering. Submonolayer amounts of Rh were deposited on the oxide films in vacuum and then the samples were exposed to NO. The reactivity was then studied as a function of Ce oxidation state, Rh coverage and temperature.

Sputtering the oxide with Ar^+ ions reduces the Ce from Ce^{4+} to Ce^{3+} and enhances the reactivity of the Rh/ CeO_2 sample. Several highly sensitive indicators of the Ce oxidation state were measured using soft x-ray photoemission (SXPS) and x-ray absorption (XAS). SXPS from the Ce 4d and Ce 4f levels and XAS at the O 1s edge are shown in Figure 24(a) to (c), respectively. These spectra were recorded at beamlines X1B and U4B. The Ce 4d spectra

are very complex and are characterized by peaks resulting from $4f^0$, $4f^1$ and $4f^2$ final states. The high binding energy peaks near 122 eV are indicative of Ce^{4+} , while peaks at lower binding energy, and in particular the shoulder at 104 eV, are characteristic of Ce^{3+} . The emission from the Ce 4f level is much easier to interpret. The Ce 4f level lies in the oxide band gap. It is unoccupied in Ce^{4+} and therefore shows very little intensity from a fully oxidized surface. The Ce 4f level is occupied in Ce^{3+} and emission from this level is evident from the sputtered surface. Finally, in the O 1s XAS spectra, hybridization between the O 2p and Ce 4f orbitals permits excitation of an O 1s electron into the Ce 4f. The peak at 530 eV results from excitation into the $4f^0$ initial state of Ce^{4+} . The resonance energy shifts to ca. 532 eV for excitation into the $4f^1$ initial state of Ce^{3+} so that the decrease in intensity at 530 eV on the sputtered surface indicates the reduction of Ce^{4+} to Ce^{3+} .

When NO is deposited on Rh on a fully oxidized CeO_2 surface at room temperature, most of the NO remains intact as indicated by N 1s SXPS and XAS. As the sample is heated, most of the NO desorbs while some dissociates into atomic N and O. On a sputtered CeO_2 surface, however, most of the NO dissociates at room temperature.